LIMOT: A Tightly-Coupled System for LiDAR-Inertial Odometry and Multi-Object Tracking

Zhongyang Zhu[1], Junqiao Zhao[*,1,2], Kai Huang[3], Xuebo Tian[1], Jiaye Lin[1], Chen Ye[1]

Abstract— Simultaneous localization and mapping (SLAM) is critical to the implementation of autonomous driving. Most LiDAR-inertial SLAM algorithms assume a static environment, leading to unreliable localization in dynamic environments. Moreover, the accurate tracking of moving objects is of great significance for the control and planning of autonomous vehicles. This study proposes LIMOT, a tightly-coupled multi-object tracking and LiDAR-inertial odometry system that is capable of accurately estimating the poses of both ego-vehicle and objects. We propose a trajectory-based dynamic feature filtering method, which filters out features belonging to moving objects by leveraging tracking results before scan-matching. Factor graph-based optimization is then conducted to optimize the bias of the IMU and the poses of both the ego-vehicle and surrounding objects in a sliding window. Experiments conducted on the KITTI tracking dataset and self-collected dataset show that our method achieves better pose and tracking accuracy than our previous work DL-SLOT and other baseline methods. Our open-source implementation is available at https://github.com/tiev-tongji/LIMOT.

I. INTRODUCTION

Simultaneous localization and mapping (SLAM) is essential for the operation of autonomous vehicles in Global Navigation Satellite System (GNSS)-denied environments. Most SLAM systems degrade in dynamic environments because they rely heavily on the assumption of a static environment. At the same time, multi-object tracking in complex dynamic scenes is crucial for the control and planning of autonomous vehicles. Therefore, approaches combining SLAM and multi-object tracking have emerged in recent years [1], [2], [3]. The vast majority of methods perform multi-object tracking and SLAM separately, i.e., loosely-coupled. This results in that the tracking accuracy highly depends on ego-pose estimation which is, however, not reliable in dynamic environments.

Recently, tightly-coupled multi-object tracking and vision-based SLAM systems have gained extensive attention [1], [4], [5], [6]. These systems construct a unified optimization framework, in which the poses of both the ego-vehicle and moving objects are jointly optimized. However, their

performance is limited by inaccurate 3D object detection and sensitivity to illumination change and rapid motion.

In this paper, we propose LIMOT, a tightly-coupled multi-object tracking and LiDAR-inertial odometry system capable of accurately estimating the poses of both the ego-vehicle and surrounding objects. First, all movable objects are detected as 3D bounding boxes. Simultaneously, inertial measurement unit (IMU) pre-integration is utilized to de-skew LiDAR scans and provide an initial guess for scan-matching. Then, similar to DL-SLOT [2], a combination of trajectory approximation of tracked objects in a sliding window and the continuous shortest path algorithm [7] is employed to perform data association. Object states (stationary or dynamic) can then be determined.

DL-SLOT filters all feature points belonging to movable objects and suffers from feature sparsity when many movable objects are actually static. However, based on the approximated object trajectories and the estimated motion from IMU pre-integration, feature points belonging to moving objects can be precisely filtered out before scan-matching in LIMOT. Finally, a factor graph optimization framework is conducted to optimize the bias of the IMU and the poses of both the ego-vehicle and objects in a sliding window. The main contributions of this work can be summarized as follows:

- Development of a tightly-coupled multi-object tracking and LiDAR-inertial odometry system, allowing for joint estimation of the poses of both the ego-vehicle and surrounding objects.
- Introduction of a method that leverages the approximated object trajectories to identify and exclude feature points belonging to moving objects, while still utilizing feature points on static movable objects to provide constraints for scan-matching.
- Extensive experiments on different datasets demonstrate the advantages of our system compared to other methods.

II. RELATED WORKS

In recent years, the multi-object tracking and SLAM system in dynamic environments has been increasingly investigated. The existing methods can be classified into two types: loosely-coupled and tightly-coupled.

In the former, multi-object tracking and SLAM are performed independently [8], [9], [10]. SLAMMOT[8] first proposed simultaneously estimating ego-motion and multi-object motion, establishing a framework to decompose the estimation problem into two separated filter-based estimators. [9] estimates ego-motion based on the static background and

[1]Zhongyang Zhu, Junqiao Zhao, Xuebo Tian, Jiaye Lin, and Chen Ye are with Department of Computer Science and Technology, School of Electronics and Information Engineering, Tongji University, Shanghai, China, and the MOE Key Lab of Embedded System and Service Computing, Tongji University, Shanghai, China (e-mail: 2233057@tongji.edu.cn; zhaojunqiao@tongji.edu.cn; 1930773@tongji.edu.cn;2310920@tongji.edu.cn; yechen@tongji.edu.cn).

[2]Institute of Intelligent Vehicles, Tongji University, Shanghai, China

[3]Kai Huang is with the School of Surveying and Geo-Informatics, Tongji University, Shanghai, China (e-mail: 1911202@tongji.edu.cn).
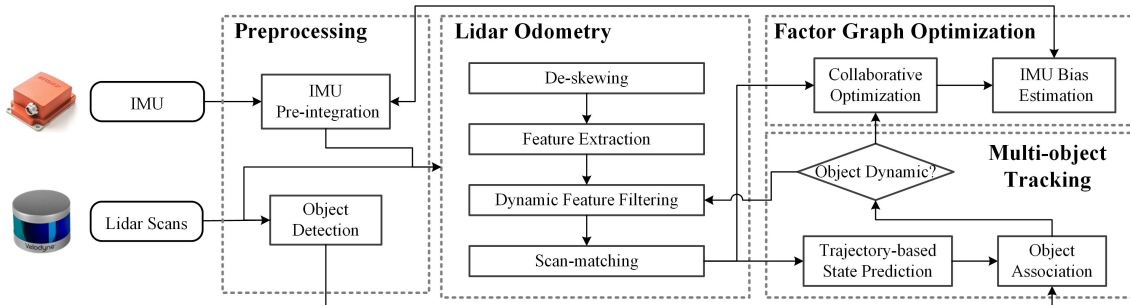
Fig. 1. The system architecture of LIMOT. The system consists of the preprocessing, LiDAR odometry, the sliding window-based 3D multi-object tracking, and factor graph optimization.

achieves object tracking through the least-squares method by fusing point clouds and 3D detection. However, the accuracy of multi-object tracking in these methods is heavily dependent on ego-pose estimation which likely fails in complex dynamic environments.

Tightly-coupled multi-object tracking and SLAM methods are primarily proposed in visual SLAM systems. Specifically, CubeSLAM [1] firstly proposed the use of a multi-view bundle adjustment (BA) to jointly optimize ego-pose, states of objects, and feature points. Dynamic objects are tracked by a 2D object tracking algorithm [11]. VDO-SLAM [4] tracks feature points on objects by leveraging dense optical flow. Motion model constraints are added to the factor graph to effectively enable the combined optimization of ego-pose and object states. DynaSLAM II [5] makes use of instance semantic segmentation and ORB feature [12] correspondences to track moving objects, jointly optimizing the static structure and trajectories of the camera and moving objects in a local-temporal window. TwistSLAM [6] achieves data association using optical flow estimation and performs a novel joint optimization by defining inter-cluster constraints modeled by mechanical joints. These vision-based methods mostly perform tracking in 2D image space and thus suffer from inaccurate 3D object detection, vulnerability to textureless or low-illumination environments, and occlusion.

Our previous work DL-SLOT [2] is, to the best of our knowledge, the first tightly-coupled LiDAR SLAM and multi-object tracking system without IMU. Recently, LIO-SEGMOT [3], proposed an optimization framework similar to ours, but without a sliding window. As a result, it is computationally expensive when there are multiple objects for tightly-coupled optimization. In addition, this method does not remove dynamic points, thus exhibiting only slight improvement in pose accuracy compared to LIO-SAM [13].

III. METHODS

A. Notation and System Overview

We consider W as the world frame and L_k as the LiDAR frames, related to the k-th LiDAR scan at time t_k, respectively. We donate $\mathbf{T}_b^a \in \mathrm{SE}(3)$ as the pose of b in frame a. We also assume that the LiDAR frame coincides with the ego-vehicle frame for convenience. Therefore, the pose of the ego-vehicle in frame W at t_k is represented as $\mathbf{T}_{L_k}^W$

and the pose transformation from t_{k-1} to t_k is represented as $\mathbf{T}_{L_k}^{L_{k-1}}$. For simplification, we denote $\mathbf{T}_{L_k}^W$ as $\mathbf{T}_k^W$ and $\mathbf{T}_{L_k}^{L_{k-1}}$ as $\mathbf{T}_k^{k-1}$. In addition, the pose of j-th object in W and the ego-vehicle frame at t_k are represented as $\mathbf{T}_{k,O_j}^W$ and $\mathbf{T}_{k,O_j}^L$, respectively. Each can be converted into the other as follows:

$$\mathbf{T}_{k,O_j}^W = \mathbf{T}_k^W \cdot \mathbf{T}_{k,O_j}^L \qquad (1)$$

An overview of the proposed system is shown in Figure 1. The system consists of four modules, Prepocessing, LiDAR Odometry, Factor Graph optimization, and Multi-object tracking, which will be detailed in the following sections.

B. Preprocessing

1) Object Detection: To simplify the object observation model, we use an open source real-time 3D LiDAR object detector CenterPoint [14] to generate the 3D bounding box and pose $\mathbf{T}_{k,O_j}^L$ of an object in LiDAR frame.

2) IMU Pre-integration: We perform IMU pre-integration to aggregate raw IMU measurements in the local frame, following [15].

C. Multi-object Tracking

We use the approach in DL-SLOT [2] to predict the position of the tracked object by fitting its trajectory in a sliding window with a cubic order polynomial. Then, a M by N matching matrix $\mathbf{\Psi}_k$ is generated by calculating the distances between the M detected objects in the current scan and the predicted positions of the N tracked objects in the previous scan. The element $\psi_k^{i,j}$ in $\mathbf{\Psi}_k$ indicates the matching score between the i-th detected object and the j-th tracked object. It can be calculated by Equation 2.

$$\psi_k^{i,j} = \begin{cases} 1 - \frac{d_{i,j}}{\alpha} & (\ d_{i,j} < d_{\mathrm{thres}}) \\ 0 & otherwise \end{cases} \qquad (2)$$

where α is a constant, $d_{i,j}$ is the distance between the detected object and the predicted position of the tracked object, and d_{thres} is the association distance threshold. The continuous shortest path algorithm [7] is employed to perform data association based on the matching matrix.

After completing the data association, the average velocities of the objects within the sliding window are calculated.

An object is determined to be dynamic when its average velocity is greater than a given threshold v_{thres}.
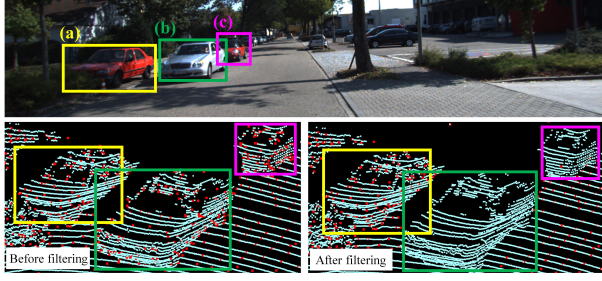
Fig. 2. Example of filtering out dynamic feature points. The light blue points denote the original point cloud and the red points denote the feature points. The feature points on the moving cars (b) and (c) are removed exactly by LIMOT, while the feature points on the static car (a) are remained.

D. LiDAR Odometry

1) De-skewing, Feature Extraction and Scan-matching: The LiDAR Odometry module is mainly inherited from LIO-SAM. For point cloud de-skewing, a nonlinear motion model is utilized with the estimated motion from the IMU, which is more precise than using a linear motion model [16]. Edge and planar feature points are then extracted based on the local roughness of the point cloud. After removing feature points belonging to moving objects (see Section III-D.2), LOAM-based scan-matching [17] is conducted between the current scan and the historical submap to obtain ego-pose $\mathbf{T}_k^W$. The initial transformation guess is obtained using the predicted ego-motion, $\widetilde{\mathbf{T}}_k^W$, from IMU pre-integration.

2) Trajectory-based Dynamic Feature Filtering: For dynamic objects at t_k, we use their fitted trajectories generated by the Multi-object tracking module to predict their positions at t_{k+1}. Based on the predicted ego-pose $\widetilde{\mathbf{T}}_{k+1}^W$ at t_{k+1}, feature points located within the 3D bounding boxes of dynamic objects can be filtered out from the $k+1$-th point cloud before scan-matching. An illustration is shown in Figure 2. There are three cars (labeled by (a), (b), and (c)) in this scene. Car (a) is parked on the side of the road, and car (b) and car (c) are traveling on the road. It can be seen that our method can filter out the feature points (shown in red) extracted from the moving objects and remain the feature points on static objects.

E. Joint Factor Graph Optimization

The joint factor graph optimization framework is shown in Figure 3. It consists of the factors providing constraints for optimization and variable nodes including the states of the ego-vehicle and surrounding objects. When an object has been tracked for 5 consecutive frames, we consider it to be initialized. Only the pose nodes of the initialized objects are added to the factor graph, which avoids false detections. We add pose nodes for initialized dynamic objects at each time t_k but maintain only one pose node in the factor graph when the object is judged as stationary to ensure the uniqueness of its global pose. This provides reliable static observation
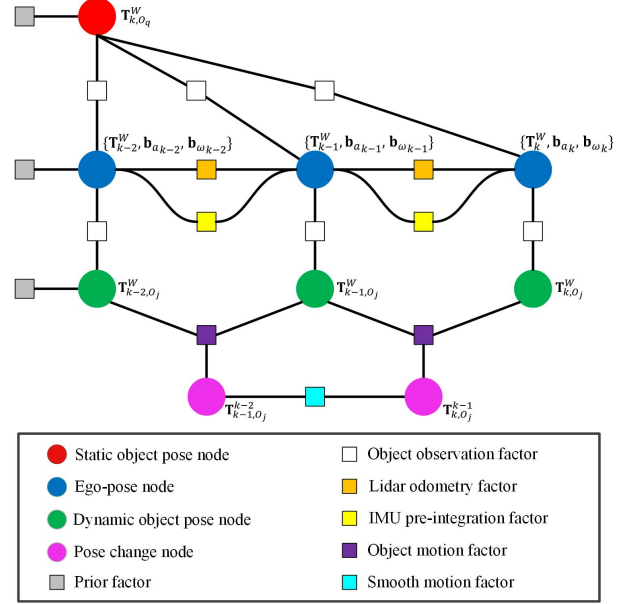
Fig. 3. Factor graph framework of LIMOT for joint optimization.

constraints. The residual formulation of each factor is given below.

Given the ego-poses at t_{k-1} and t_k estimated by LiDAR scan-matching, the residual of the LiDAR odometry factor can be defined as follows:

$$\mathbf{r}_{odo}^k(\mathbf{T}_{k-1}^W, \mathbf{T}_k^W) = (\mathbf{T}_{k-1}^{W}{}^{-1} \cdot \mathbf{T}_k^W) \cdot \mathbf{T}_k^{k-1}{}^{-1} \quad (3)$$

Then, based on the object detection results, the residual of the object observation factor is defined as follows:

$$\mathbf{r}_{obs}^{k,j}(\mathbf{T}_k^W, \mathbf{T}_{k,O_j}^W) = (\mathbf{T}_k^{W}{}^{-1} \cdot \mathbf{T}_{k,O_j}^W) \cdot \mathbf{T}_{k,O_j}^{L}{}^{-1} \quad (4)$$

The pose change of object $\mathbf{T}_{k,O_j}^{k-1}$ between t_{k-1} and t_k can be calculated using Equation 5, which also indicates the velocity of the object.

The object motion factor is a ternary factor associated with three nodes: two dynamic object pose nodes $\mathbf{T}_{k-1,O_j}^W$, $\mathbf{T}_{k,O_j}^W$ and one pose change node $\mathbf{T}_{k,O_j}^{k-1}$. These are continually updated throughout the optimization process, but they must always satisfy Equation 5. Thus, the residual of the object motion factor is defined by Equation 6.

$$\mathbf{T}_{k,O_j}^{k-1} = \mathbf{T}_{k-1,O_j}^{W}{}^{-1} \cdot \mathbf{T}_{k,O_j}^W \quad (5)$$

$$\mathbf{r}_{moti}^{k,j}(\mathbf{T}_{k-1,O_j}^W, \mathbf{T}_{k,O_j}^W, \mathbf{T}_{k,O_j}^{k-1}) = (\mathbf{T}_{k-1,O_j}^{W}{}^{-1}\cdot\mathbf{T}_{k,O_j}^W)\cdot\mathbf{T}_{k,O_j}^{k-1}{}^{-1} \quad (6)$$

We assume that a dynamic object moves at a constant velocity over a short period of time, such that the pose changes of the object at successive times should be almost identical. Therefore, the residual of the smooth motion factor is defined as:

$$\mathbf{r}_{smoo}^{k,j}(\mathbf{T}_{k-1,O_j}^{k-2}, \mathbf{T}_{k,O_j}^{k-1}) = \mathbf{T}_{k-1,O_j}^{k-2}{}^{-1} \cdot \mathbf{T}_{k,O_j}^{k-1} \quad (7)$$

Finally, the optimization problem can be denoted as:

Seq	LIO-SAM [13] ATE$_T$[m]	ATE$_R$[rad]	DL-SLOT [2] ATE$_T$[m]	ATE$_R$[rad]	LIO-SEGMOT [3] ATE$_T$[m]	ATE$_R$[rad]	LIO-Allfilt ATE$_T$[m]	ATE$_R$[rad]	LIO-Dynafilt ATE$_T$[m]	ATE$_R$[rad]	LIMOT ATE$_T$[m]	ATE$_R$[rad]
00	0.856	0.024	0.984	0.031	0.867	**0.020**	0.854	0.024	0.852	0.024	**0.846**	0.024
01	1.683	0.044	1.764	0.193	1.704	**0.043**	1.824	**0.043**	1.686	0.044	**1.681**	0.045
02	0.274	0.013	0.362	0.023	**0.253**	0.016	0.280	0.014	0.274	**0.012**	0.269	0.013
03	**0.245**	0.031	1.920	0.050	0.269	0.038	0.247	**0.028**	0.246	**0.028**	**0.245**	0.030
04	0.660	0.104	1.050	0.276	0.657	0.114	0.659	0.116	0.634	0.099	**0.629**	0.107
05	0.347	0.134	1.209	**0.100**	**0.313**	0.124	0.346	0.127	0.342	0.122	0.355	0.112
06	0.266	0.013	1.925	**0.081**	0.202	0.012	0.199	0.012	0.206	0.012	**0.190**	0.012
07	1.319	0.025	1.759	0.272	1.376	0.032	1.331	0.025	1.308	**0.024**	1.278	**0.024**
08	1.274	0.307	2.807	**0.284**	**1.120**	**0.284**	1.253	0.328	1.257	0.310	1.237	0.311
09	1.201	**0.024**	1.597	1.123	**1.135**	0.025	1.181	**0.024**	1.220	0.025	1.175	0.030
10	0.438	0.108	0.860	0.137	0.495	**0.106**	0.447	0.118	0.438	**0.106**	0.425	**0.106**
11	0.262	0.202	0.303	0.214	0.282	0.283	**0.260**	0.182	0.262	0.150	0.266	0.181
13	0.260	0.044	0.331	0.051	0.258	**0.040**	0.263	0.043	0.262	0.043	**0.256**	0.045
14	0.105	0.013	0.151	0.197	**0.095**	0.013	0.111	0.014	0.107	0.013	0.108	**0.012**
15	0.275	0.066	0.385	**0.012**	0.291	0.076	0.274	0.065	**0.273**	0.066	0.274	0.066
18	0.385	**0.141**	0.851	0.166	**0.371**	0.168	0.374	0.157	0.376	0.159	0.373	0.160
19	0.916	0.122	1.006	0.358	0.955	0.136	0.916	0.131	0.916	0.135	**0.915**	**0.120**
20	9.488	**0.021**	22.349	0.043	9.313	0.023	1.863	0.027	1.834	0.025	**1.710**	0.027
mean	1.125	0.080	2.312	0.201	1.109	0.086	0.705	0.082	0.694	**0.078**	**0.680**	0.079

$$
\mathcal{X}^* = \underset{\mathcal{X}}{argmin} \Big\{ \|\mathbf{r}_P(\mathcal{X})\|^2 + \sum_{k \in \mathcal{I}} \left\| \mathbf{r}_I^k(\mathcal{X}) \right\|_{Q_I}^2
$$

$$
+ \sum_{k \in \mathcal{L}} \big(\left\| \log(\mathbf{r}_{odo}^k(\mathcal{X})) \right\|_{Q_{odo}}^2 + \sum_{j \in \mathcal{O}_k} (\left\| \log(\mathbf{r}_{obs}^{k,j}(\mathcal{X})) \right\|_{Q_{obs}}^2
$$

$$
+ \left\| \log(\mathbf{r}_{moti}^{k,j}(\mathcal{X})) \right\|_{Q_{moti}}^2 + \left\| \log(\mathbf{r}_{smoo}^{k,j}(\mathcal{X})) \right\|_{Q_{smoo}}^2)) \Big\}
$$

(8)

where $\mathcal{X}$ is the set of all variables, $\|\mathbf{r}_P(\mathcal{X})\|^2$ is the prior from marginalization, $\mathcal{I}$ is the set of all IMU measurements, $\mathcal{L}$ is the set of LiDAR scans in the sliding window, and Q represents the covariance matrix. $\mathbf{r}_I^k(\mathcal{X})$ is the formula of the IMU pre-integration factor residual. The operation $\log()$ represents the transformation from SE(3) to $\mathfrak{se}(3)$. Each LiDAR scan is related to the tracked object set $\mathcal{O}_k$.

IV. EXPERIMENTS

We conducted experiments using the public KITTI tracking dataset [18] and the self-collected dataset to evaluate the performance of the proposed LIMOT. All experiments were based on real-time detection results from CenterPonit, whose weights are trained on the Argoverse 2 dataset [19]. For all the experiments, we set the sliding window size to 5, v_{thres} to 1 m/s, and α to 100. Additionally, the d_{thres} for initialized object association was set to 2 m. Experiments were carried out on a workstation with Ubuntu 20.04, equipped with an Intel Core Xeon(R) Gold 6248R 3.00GHz processor, 32G RAM, and a NVIDIA RTX A4000 16GB graphic card.

A. Evaluation Metrics

The root-mean-square error (RMSE) of the translational and the rotational absolute trajectory errors (ATE$_T$ [m] and ATE$_R$ [rad]) are adopted to assess the accuracy of ego-poses [20]. The performance of multi-object tracking is evaluated in two ways following [5]. The pose accuracy of the objects is also evaluated using the RMSE of ATE$_T$ [m] and ATE$_R$ [rad]. The multi-object tracking precision (MOTP) metric [21] is used to evaluate tracking precision. MOTP results are only given on the KITTI tracking dataset since it provides the ground truth tracking results for evaluation.

B. Baselines

The baseline multi-object tracking and SLAM methods are DL-SLOT [2] and LIO-SEGMOT [3]. LIO-SAM [13] is also compared since it is one of the state-of-the-art (SOTA) LiDAR-inertial SLAM methods, on which we build LIMOT. When only the proposed dynamic feature point removal is performed without joint optimization, the method is referred to as LIO-Dynafilt. In addition, we also provide experimental results of removing all feature points on movable objects without joint optimization, LIO-Allfilt.

We selected two popular 3D multi-object tracking methods, AB3DMOT [22] and PC3T [23], as well as DL-SLOT and LIO-SEGMOT as the baseline multi-object tracking methods. AB3DMOT first proposed to directly evaluate multi-object tracking in 3D space, which is suitable for LiDAR-based approaches. PC3T is a SOTA multi-object tracking method that requires ground truth ego-poses as input.

C. KITTI Tracking Dataset

1) Ego-pose Evaluation: The KITTI tracking dataset was collected in urban areas and along highways. We chose all the sequences in the KITTI tracking dataset except for sequences without ego-motion. The comparative results are shown in Table I. LIO-Allfilt shows a large translational error in sequence 01 because parked cars are representative in this sequence. The filtering of all their feature points impedes scan-matching. The pose accuracy of LIO-Dynafilt is higher than those of LIO-SAM and LIO-Allfilt, demonstrating the
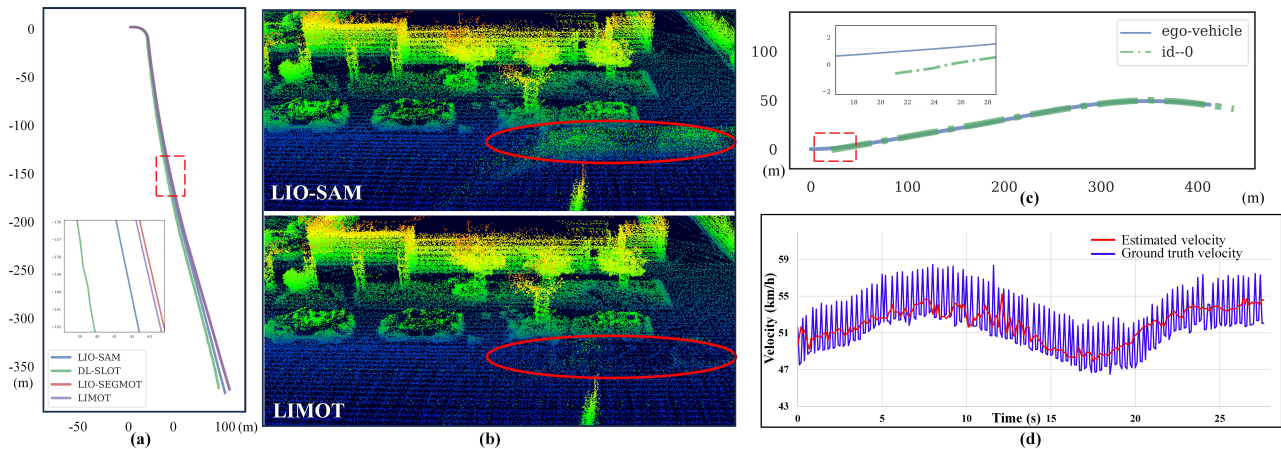
Fig. 4. Qualitative results of LIMOT on the KITTI tracking dataset. (a) Comparison of ego-trajectories in sequence 04 of the KITTI tracking dataset. (b) Comparison of point cloud maps generated by LIO-SAM and LIMOT. (c) Trajectories of the main tracked object (id 0) and ego-vehicle in sequence 10 of the KITTI tracking dataset. (d) Comparison between the ground truth and estimated instantaneous velocity of the tracked object in (c).

TABLE II

MOTP [%] RESULT COMPARISON OF DIFFERENT MULTI-OBJECT TRACKING ALGORITHMS ON THE KITTI TRACKING DATASET

Method	MOTP [%]	
	(IOU$_{thres}$ = 0.25)	(IOU$_{thres}$ = 0.5)
AB3DMOT	61.37	64.17
PC3T	61.26	64.07
DL-SLOT	60.13	63.60
LIO-SEGMOT	61.45	64.22
LIMOT	**62.25**	**64.26**

effectiveness of our proposed dynamic feature filtering approach. Compared to DL-SLOT, all other methods achieve better performance, demonstrating that coupling IMU assists in localization. LIMOT achieves the best pose estimation performance in many of the evaluated sequences, confirming that jointly optimizing the poses of the ego-vehicle and objects is beneficial. LIO-SEGMOT does not improve the pose accuracy much compared to LIO-SAM because it does not consider the effect of dynamic features on the scan-matching. It is important to note that sequence 20 is a highway scene containing a large number of moving objects, so LIMOT, LIO-Dynafilt, and LIO-Dynafilt all have a large improvement compared to LIO-SAM and LIO-SEGMOT. Moreover, since the highway is a typical scene for LiDAR SLAM degradation, DL-SLOT shows the largest translational error.

The comparison of ego-trajectories of sequence 04 is shown in Figure 4 (a). The point cloud maps of sequence 01 generated by LIO-SAM and LIMOT are shown in Figure 4 (b). In the red ellipse of the former, there is a very obvious ghosting caused by the moving objects, which, however, is eliminated from the point cloud generated by LIMOT.

2) Tracking Precision Evaluation: The comparison results are shown in Table II. For each tracked object, its Intersection over Union (IoU) with ground truth label should exceed a threshold IoU$_{thres}$ to be considered as a successful match.

It can be found that our method shows the best results in terms of MOTP, indicating that our method achieves better tracking precision for all tracked objects.

3) Object Pose Evaluation: We further evaluated the pose accuracy of the individual objects. We selected 10 objects with the longest tracking frame length in Table I for evaluation. The experimental results are shown in Table III. Here TP [%] stands for the ratio of the number of tracked frames to the number of the frames of the object's ground truth trajectory. The IoU threshold for evaluating TP is taken as 0.25. Since we adopt the tracking method in DL-SLOT, the TP results of these two methods are the same on most sequences. However, the pose accuracy of objects is improved significantly in LIMOT, largely due to the reduction of the ego-pose rotation error by coupling IMU measurements. Moreover, LIMOT and LIO-SEGMOT track the objects for almost the same number of frames, but LIMOT achieves better pose accuracy of the objects.

The trajectories of the tracked object (id 0) and ego-vehicle in sequence 10 are demonstrated in Figure 4 (c). We further compare the estimated instantaneous velocity of the object (id 0) in sequence 10 with the ground truth. As shown in Figure 4 (d), the ground truth instantaneous velocities (blue line) exhibit significant fluctuation due to the imprecise object annotations within the dataset. In contrast, the estimated instantaneous velocities by LIMOT (red line) are smoother and in the middle of the fluctuation range of the ground truth. This indicates that it is appropriate to add the constant velocity constraint to the factor graph optimization.

D. Self-collected Dataset

1) Data Collection: We collected this dataset using the TIEV platform [24] on the North Jiasong Road, Jiading District, Shanghai. Figure 5 shows an overview of this dataset and it can be seen that this scene is rich in dynamic objects. TIEV is equipped with a Velodyne HDL-64E LiDAR and an RTK-Inertial Navigation System (INS), which provides IMU data at 100 HZ as well as high-precision ground truth.

TABLE III

Seq / Obj.id	DL-SLOT [2]			LIO-SEGMOT [3]			LIMOT		
	TP [%]	ATE_T[m]	ATE_R[rad]	TP [%]	ATE_T[m]	ATE_R[rad]	TP [%]	ATE_T[m]	ATE_R[rad]
04 / 2	27.07	2.799	1.760	**27.71**	0.711	0.241	27.07	**0.697**	**0.233**
05 / 31	**40.40**	0.924	0.223	40.07	0.304	0.175	40.40	0.302	**0.163**
08 / 8	23.33	0.661	0.346	**24.36**	0.430	**0.122**	23.08	**0.384**	0.130
08 / 13	48.85	0.827	0.116	**50.76**	0.656	**0.104**	48.85	0.641	0.105
10 / 0	**93.88**	0.943	0.168	88.44	0.439	**0.156**	93.88	**0.368**	0.156
11 / 0	**51.21**	0.445	**0.129**	50.40	0.292	0.186	51.21	**0.277**	0.189
18 / 2	29.17	0.566	0.878	**31.44**	**0.246**	**0.580**	30.68	0.261	0.602
18 / 3	46.67	0.493	**0.456**	45.61	0.386	0.560	**47.02**	0.372	0.459
20 / 12	37.79	10.342	0.106	45.10	1.701	0.105	**46.66**	**0.826**	**0.102**
20 / 122	**30.20**	1.005	**0.117**	29.41	**0.258**	0.127	30.20	0.292	0.131
mean	42.86	1.901	0.430	43.33	0.542	0.236	**43.90**	**0.442**	**0.227**
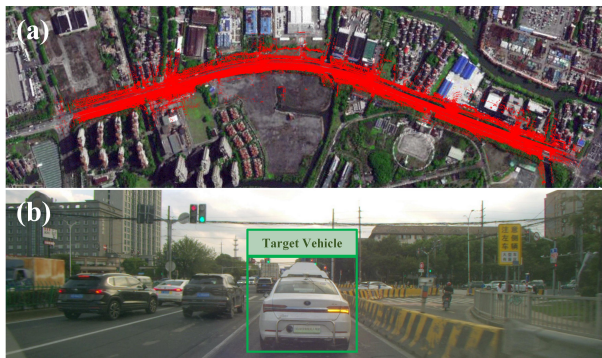
Fig. 5. The overview of the self-collected dataset. (a) LIMOT mapping result aligning with the satellite map. (b) A representative front view image of the self-collected dataset.

TABLE IV

RESULTS OF POSE ESTIMATION COMPARISON ON THE SELF-COLLECTED DATASET. BOLD AND UNDERLINED TEXT INDICATE THE BEST AND THE SUBOPTIMAL RESULT, RESPECTIVELY

Method	Ego-pose		Target object pose		
	ATE_T[m]	ATE_R[rad]	TP [%]	ATE_T[m]	ATE_R[rad]
LIO-SAM	3.344	0.049	–	–	–
DL-SLOT	5.188	0.118	68.61	0.524	0.092
LIO-SEGMOT	3.243	**0.046**	**85.99**	2.593	**0.079**
LIO-Allfilt	3.358	**0.046**	–	–	–
LIO-Dynafilt	3.314	0.047	–	–	–
LIMOT	**3.005**	**0.046**	71.73	**0.212**	0.092

In addition, we used a target vehicle, playing the role of the tracked object, equipped with the same INS, so we can obtain its ground truth trajectory.

2) Pose Evaluation: Both the ego-vehicle and the target vehicle pose evaluation results are shown in Table IV. Compared to LIO-SAM, the ego-pose result of LIMOT presents in an average improvement of 10.14% and 6.12% in terms of ATE_T and ATE_R, respectively. As for the target object pose result, although LIO-SEGMOT tracks the object for a longer period of time, it shows a significant translational error. LIMOT obtains the most accurate target object position.

TABLE V

AVERAGE TIME-CONSUMING OF THE MAIN FUNCTIONAL MODULES FOR PROCESSING ONE SCAN

Module	Average Runtime (ms)
LiDAR Odometry	78.4 + 0.4
Multi-object Tracking	0.9
Factor Graph Optimization	1.5 + 7.4

	LIO-SAM	LIO-SEGMOT	LIMOT
FPS	12.6	7.5	11.3

E. Running Time Analysis

We calculated the average time-consumption of the main functional modules of LIMOT on the KITTI tracking dataset. The results are shown in Table V. Compared with LIO-SAM, the time consumption of LiDAR odometry and factor graph optimization increase by 0.4 ms and 7.4 ms, respectively, which correspond to the runtime of the dynamic feature filtering and joint optimization of the states of objects. LIO-SEGMOT performs significantly slower than LIMOT because of its computationally intensive factor graph structure.

V. CONCLUSIONS

We present LIMOT, a tightly-coupled system for LiDAR-inertial SLAM and multi-object tracking capable of jointly optimizing the poses of the ego-vehicle and objects in a sliding window. Furthermore, this method can filter out feature points on moving objects based on the approximated object trajectories, while the remaining feature points on static objects are used to provide constraints for scan-matching, which enhances the robustness of the system and improves its performance in dynamic environments. Experimental results show that LIMOT improves the pose accuracy of ego-vehicle and objects, as well as the tracking accuracy, which demonstrates that LiDAR-inertial SLAM and multi-object tracking can exhibit mutual benefits on each other. Future work could involve introducing a dynamics model for moving objects in the environment to obtain more accurate object states.

REFERENCES

[1] S. Yang and S. Scherer, "Cubeslam: Monocular 3-d object slam," *IEEE Transactions on Robotics*, vol. 35, no. 4, pp. 925–938, 2019.

[2] X. Tian, Z. Zhu, J. Zhao, G. Tian, and C. Ye, "Dl-slot: Dynamic lidar slam and object tracking based on collaborative graph optimization," *arXiv preprint arXiv:2212.02077*, 2022.

[3] Y.-K. Lin, W.-C. Lin, and C.-C. Wang, "Asynchronous state estimation of simultaneous ego-motion estimation and multiple object tracking for lidar-inertial odometry," pp. 1–7, 2023.

[4] J. Zhang, M. Henein, R. Mahony, and V. Ila, "Vdo-slam: a visual dynamic object-aware slam system," *arXiv preprint arXiv:2005.11052*, 2020.

[5] B. Bescos, C. Campos, J. D. Tardós, and J. Neira, "Dynaslam ii: Tightly-coupled multi-object tracking and slam," *IEEE Robotics and Automation Letters*, vol. 6, no. 3, pp. 5191–5198, 2021.

[6] M. Gonzalez, E. Marchand, A. Kacete, and J. Royan, "Twistslam: Constrained slam in dynamic environment," *IEEE Robotics and Automation Letters*, vol. 7, no. 3, pp. 6846–6853, 2022.

[7] R. K. Ahuja, T. L. Magnanti, and J. B. Orlin, "Network flows," 1988.

[8] C.-C. Wang, C. Thorpe, S. Thrun, M. Hebert, and H. Durrant-Whyte, "Simultaneous localization, mapping and moving object tracking," *The International Journal of Robotics Research*, vol. 26, no. 9, pp. 889–916, 2007.

[9] T. Ma and Y. Ou, "Mlo: Multi-object tracking and lidar odometry in dynamic envirnoment," *arXiv preprint arXiv:2204.11621*, 2022.

[10] M. Runz, M. Buffier, and L. Agapito, "Maskfusion: Real-time recognition, tracking and reconstruction of multiple moving objects," in *2018 IEEE International Symposium on Mixed and Augmented Reality (ISMAR)*. IEEE, 2018, pp. 10–20.

[11] J. F. Henriques, R. Caseiro, P. Martins, and J. Batista, "High-speed tracking with kernelized correlation filters," *IEEE transactions on pattern analysis and machine intelligence*, vol. 37, no. 3, pp. 583–596, 2014.

[12] E. Rublee, V. Rabaud, K. Konolige, and G. Bradski, "Orb: An efficient alternative to sift or surf," in *2011 International conference on computer vision*. Ieee, 2011, pp. 2564–2571.

[13] T. Shan, B. Englot, D. Meyers, W. Wang, C. Ratti, and D. Rus, "Lio-sam: Tightly-coupled lidar inertial odometry via smoothing and mapping," in *2020 IEEE/RSJ international conference on intelligent robots and systems (IROS)*. IEEE, 2020, pp. 5135–5142.

[14] T. Yin, X. Zhou, and P. Krahenbuhl, "Center-based 3d object detection and tracking," in *Proceedings of the IEEE/CVF conference on computer vision and pattern recognition*, 2021, pp. 11 784–11 793.

[15] C. Forster, L. Carlone, F. Dellaert, and D. Scaramuzza, "On-manifold preintegration for real-time visual–inertial odometry," *IEEE Transactions on Robotics*, vol. 33, no. 1, pp. 1–21, 2016.

[16] H. Ye, Y. Chen, and M. Liu, "Tightly coupled 3d lidar inertial odometry and mapping," in *2019 International Conference on Robotics and Automation (ICRA)*. IEEE, 2019, pp. 3144–3150.

[17] J. Zhang and S. Singh, "Loam: Lidar odometry and mapping in real-time," in *Proceedings of Robotics: Science and Systems Conference*, June 2014.

[18] A. Geiger, P. Lenz, and R. Urtasun, "Are we ready for autonomous driving? the kitti vision benchmark suite," in *Conference on Computer Vision and Pattern Recognition (CVPR)*, 2012.

[19] B. Wilson, W. Qi, T. Agarwal, J. Lambert, J. Singh, S. Khandelwal, B. Pan, R. Kumar, A. Hartnett, J. K. Pontes, *et al.*, "Argoverse 2: Next generation datasets for self-driving perception and forecasting," *arXiv preprint arXiv:2301.00493*, 2023.

[20] Z. Zhang and D. Scaramuzza, "A tutorial on quantitative trajectory evaluation for visual (-inertial) odometry," in *2018 IEEE/RSJ International Conference on Intelligent Robots and Systems (IROS)*. IEEE, 2018, pp. 7244–7251.

[21] K. Bernardin and R. Stiefelhagen, "Evaluating multiple object tracking performance: the clear mot metrics," *EURASIP Journal on Image and Video Processing*, vol. 2008, pp. 1–10, 2008.

[22] X. Weng, J. Wang, D. Held, and K. Kitani, "Ab3dmot: A baseline for 3d multi-object tracking and new evaluation metrics," *arXiv preprint arXiv:2008.08063*, 2020.

[23] H. Wu, W. Han, C. Wen, X. Li, and C. Wang, "3d multi-object tracking in point clouds based on prediction confidence-guided data association," *IEEE Transactions on Intelligent Transportation Systems*, vol. 23, no. 6, pp. 5668–5677, 2021.

[24] J. Zhao, C. Ye, Y. Wu, L. Guan, L. Cai, L. Sun, T. Yang, X. He, J. Li, Y. Ding, *et al.*, "Tiev: The tongji intelligent electric vehicle in the intelligent vehicle future challenge of china," in *2018 21st International Conference on Intelligent Transportation Systems (ITSC)*. IEEE, 2018, pp. 1303–1309.